The University of Saskatchewan
Department of Computer Science

Technical Report #2010-03

UNIVERSITY OF
SASKATCHEWAN

Modeling and Simulation of the CLS Cryogenic System

Veeramani Chidambaranathan and Raymond J. Spiteri

November 12, 2010

Abstract

This paper presents results pertaining to the numerical modeling of the cryogenic system at the Canadian Light Source. The cryogenic system consists of the cryostat that houses a Radio Frequency (RF) Cavity used for boosting energy of an electron beam. For consistent operation of the RF Cavity, it must be kept immersed in liquid helium at a constant level with the pressure in the gas space maintained to an accuracy of ± 1 mbar. The numerical method developed for solving the cryostat model [5] along with the liquid helium supply and gaseous helium return lines is validated using two different validation cases, viz., the liquid helium flow rate from the liquid helium transfer line and the gaseous helium flow rate from the cryostat for various heater power input settings. The numerical method described here is significantly more accurate and efficient than that used in [6].

1 Introduction

The Canadian Light Source (CLS) is a unique research facility in Canada that produces extremely bright light in a synchrotron. The electron beam used for this purpose loses energy with every photon emitted, but it is re-energized in a Radio Frequency (RF) cavity made of niobium that is maintained in a superconducting state using liquid helium at 4.5 K. Maintaining this low temperature requires accurate control of the pressure and level of liquid helium in the cryostat that houses the RF cavity. We wish to simulate the process equipment that makes up the cryogenic system in order to gauge the sensitivity of the pressure and level of liquid helium to changes in the control valve opening. In this report, we present the mathematical formulation and results of dynamic simulations of the cryostat in the cryogenic system using a control-volumes approach.

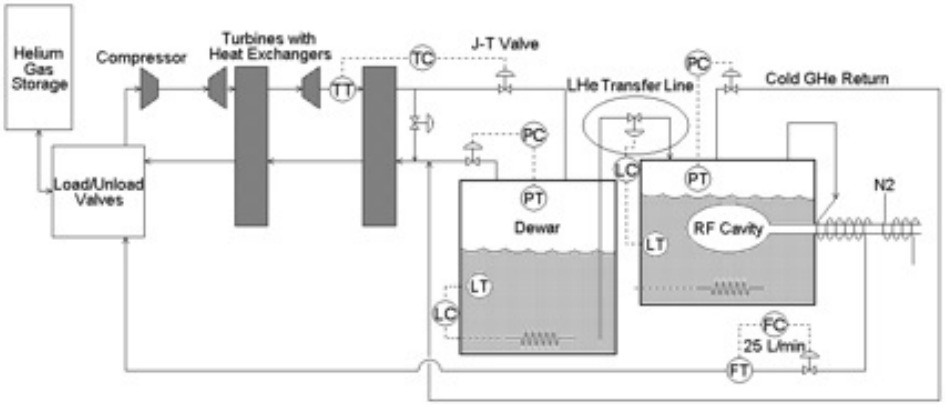

Figure 1: Process flow diagram of the cryogenic system at the CLS.

1.1 The process description

As depicted in Figure 1, gaseous helium (GHe) is compressed and cooled to 10 K by compressors and turbines with heat exchangers. Further cooling is achieved through the Joule–Thomson effect by expansion through a valve. The liquid helium (LHe) is collected in a vessel called a *dewar*. The pressure and liquid level in the dewar are maintained by standard PI controllers. The pressure controller returns cold GHe through turbine heat exchangers. The normal operating pressure in the dewar is 1.37 bars, with corresponding saturation temperature of 4.5 K; however it may vary between 1.35 to 1.38 bars. The liquid level in the dewar is maintained using resistor heating, which activates if the level becomes too high. This resistor and the Joule–Thomson valve position are used in conjunction with a level and a pressure transmitter to maintain the LHe level and pressure in the dewar.

The RF cavity is housed inside the cryostat, which is equipped with a level controller and a pressure controller. Similar to situation in the dewar, the pressure controller maintains a set pressure by returning cold GHe to the heat exchangers. The normal operating pressure in the cryostat is 1.22 bars, corresponding to a saturation temperature of 4.4 K; however it may vary between 1.19 to 1.23 bars. The LHe delivered from the dewar to the cryostat is expected to boil off in the cryostat, thus cooling the LHe in the cryostat. There is power dissipation into the cryostat from three sources, namely, the RF cavity, the heating resistor that is used to maintain liquid level, and static heat loading into the system through various instruments. The liquid level is regulated by a control valve on the LHe transfer line from the dewar. Another GHe line is withdrawn from the cryostat to keep the waveguide cold. The waveguide is the energy transfer device to the RF cavity that must be protected from thermal shock because part of it is inside the cryostat and

part is at room temperature (∼300 K). Further, a liquid nitrogen line is also used in cooling the waveguide. The GHe drawn from the cryostat is at a set flow rate of 25 L/min, controlled by a flow controller. Note that this flow rate is measured at room temperature; at the conditions in the cryostat, the flow is negligible (0.2% of the overall flow through the cryostat).

1.2 Outline of this report

The operation of the cryostat has to be at a consistent set pressure for the RF Cavity to produce an electron beam of consistent energy. The chattering of control valves or formation of two phases in the LHe transfer line can cause pressure fluctuations in the cryostat. The scope of the project is to model the system to understand the source of pressure fluctuations in the transfer line, potentially due to two-phase formation or sensitivity of the system to control valve operations. This could lead to various levels of process modification. Near-term modifications may include changing the operating conditions or the control valves and their operation method, e.g., pneumatically operated or electrically motorized operation. In the long term, the effects of dramatic process changes such as

- shortening the length of transfer line by moving the dewar closer to the cryostat
- adding a standby set of dewar and cryostat to avoid shutdown

could be studied based on this work.

A one-dimensional homogeneous flow model coupled with thermodynamic properties model for helium has been developed in [6]. The corresponding code was developed in MATLAB^{TM}. This work presents a more efficient and more accurate computational approach based on control-volume balances for steady-state flow to predict the void fractions, velocity, and liquid flow rate in the transfer line. A similar approach is adapted to predict the pressure, temperature, and velocity in gas return line.

The pipeline geometry modeled is presented in Section 2, followed by the lumped system model based on control-volumes approach in Section 3 for the LHe transfer line and Section 4 for the GHe return line.

The heat loading on the LHe transfer line and the GHe return line is of special importance and is discussed in Section 5.

Unlike the pipelines, which are modeled as stationary lumped systems, the cryostat that houses the RF Cavity is modeled as a dynamic system in order to capture the fluctuations in pressure and level. The details of the cryostat model is discussed in Section 6.

The model equations, their implementation and the numerical schemes employed to solve the cryostat along with controllers, liquid supply line, and gas return line are discussed in Section 7.

The results of the lumped system model and the one-dimensional homogeneous model are compared in Section 8. We discuss two validation cases: one for the liquid flow rate from the LHe transfer line and another for the dynamics of cryostat operation along with heater input and pressure and level control valve operation in addition to the LHe supply and GHe return flow rates.

Finally, the key contributions are listed in Section 9. The model presented forms the basis of future work that could include the compressors, turbines, process vessels, viz., the cryostat and the dewar, and the complete process line network along with the controllers for a full system simulation of cryogenic system at the CLS.

2 The Pipeline Geometry

The pipeline network currently modeled includes the LHe transfer line from the dewar to the cryostat and the GHe return lines, namely, the GHe return from the cryostat to the T-junction, the GHe return from the dewar to the T-junction, and the combined GHe line after the T-junction across the heat exchangers up to the suction of compressors, as shown in Figure 2. The LHe line has a level control valve that is regulated by a proportional-integral controller based on the signal from the level transmitter in the cryostat. The GHe return line has a pressure control valve that is regulated by a proportional-integral controller based on the signal from the pressure transmitter in the cryostat and a cold return valve (CRV) that diverts flow to heat exchanger if the temperature of the GHe is below a certain set limit; otherwise the GHe passes through the warm return valve for further cooling.

The various sections of the LHe line from the dewar to the cryostat appear in Table 1. A similar break-down of the sections in the GHe line appears in Table 2.

The pipes carrying LHe from the dewar to the cryostat and the GHe return from the cryostat to the cold box are enclosed in vacuum-jacketed (VJ) pipe and are further protected by a liquid nitrogen shield. The outer diameter of the LHe line is 0.5”, with a wall thickness of 0.049”, assumed to be same throughout its length. For the GHe return line from the cryostat to the T-junction, a constant diameter of 0.902” is assumed. The GHe line from the dewar has a diameter of 0.622”, and the line after the T-junction is 1.049”, expanding to 4.026” at the compressor suction.

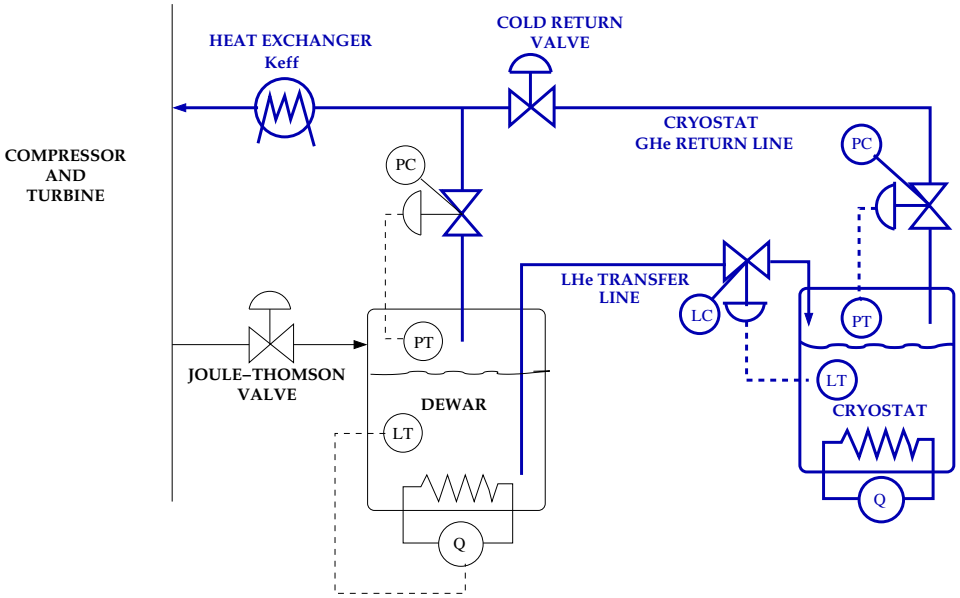

Figure 2: The part of the process flow of the cryogenic system modeled.

Line Orientation	Line length (m)	End Position (m)	Location
Vertical upflow	1.75	1.75	Vertical exit inside dewar
Flexible loose coil, 45° incline	2.54	4.29	Vacuum between outer (2.5”) and inner (0.5”) braided steel lines
Horizontal	52.10	56.39	Inside VJ line
Elevation drop of 1.5 m	1.21	57.60	Inside valve box
Flexible loose coil, 45° incline	2.63	60.23	Vacuum between outer (ID 1.5” and OD 2.25”) and inner (ID 0.5” and OD 0.75”)
Vertical downflow	0.1	60.33	Vertical entrance inside cryostat

Table 1: The various sections in the LHe transfer line.

Line Orientation	Line length (m)	End Position (m)	Location
Segment-1: From Cryostat to T-junction			
Flexible loose coil 45° incline	2.63	2.63	From cryostat to cold valve box inside 3" vaccuum line
Vertical rise of 1.5 m (assumed)	3.72	6.35	Inside valve box contains the venturi meter and pressure control valve
Vertical rise of 0.2 m	0.2	6.55	VJ line from valve box to horizontal portion
Horizontal	49.33	55.88	Inside VJ line
Vertical downflow	2.08	57.96	Vertical end VJ line
Flexible loose coil, 45° incline	3.54	61.5	0.75" contained in 2.5" vaccuum line
Horizontal run before CRV	0.5	62.0	Inside cold box
Horizontal run after CRV to T-junction	0.5	62.5	Inside cold box
Segment-2: From Dewar to T-junction			
Vertical rise	1.01	1.01	Vertically above dewar
Horizontal	1.5	2.51	Horizontal section to the cold box
Vertical downflow	1.09	3.60	Inside cold box
Horizontal run to the T-junction	0.5	4.1	Inside cold box
Segment-3: From T-junction to the compressor suction			
Across the heat exchanger	1.0	1.0	Inside cold box (assumed)

Table 2: The various sections in the GHe return network.

The pipe fittings on the VJ line that give frictional pressure losses are given in Table 3. The positions of the fittings for the LHe line are given with respect to the origin at the dewar inlet, whereas the position of fittings for the GHe line are given with respect to the origin at the cryostat inlet. The fittings numbered 4 to 15 are the same fittings that are referenced with respect to different origins. The loss coefficients are different due to different sizes of the LHe and GHe lines. The fittings on the GHe segments connecting the dewar to the cold box and from T-junction to the compressors are given in Table 4.

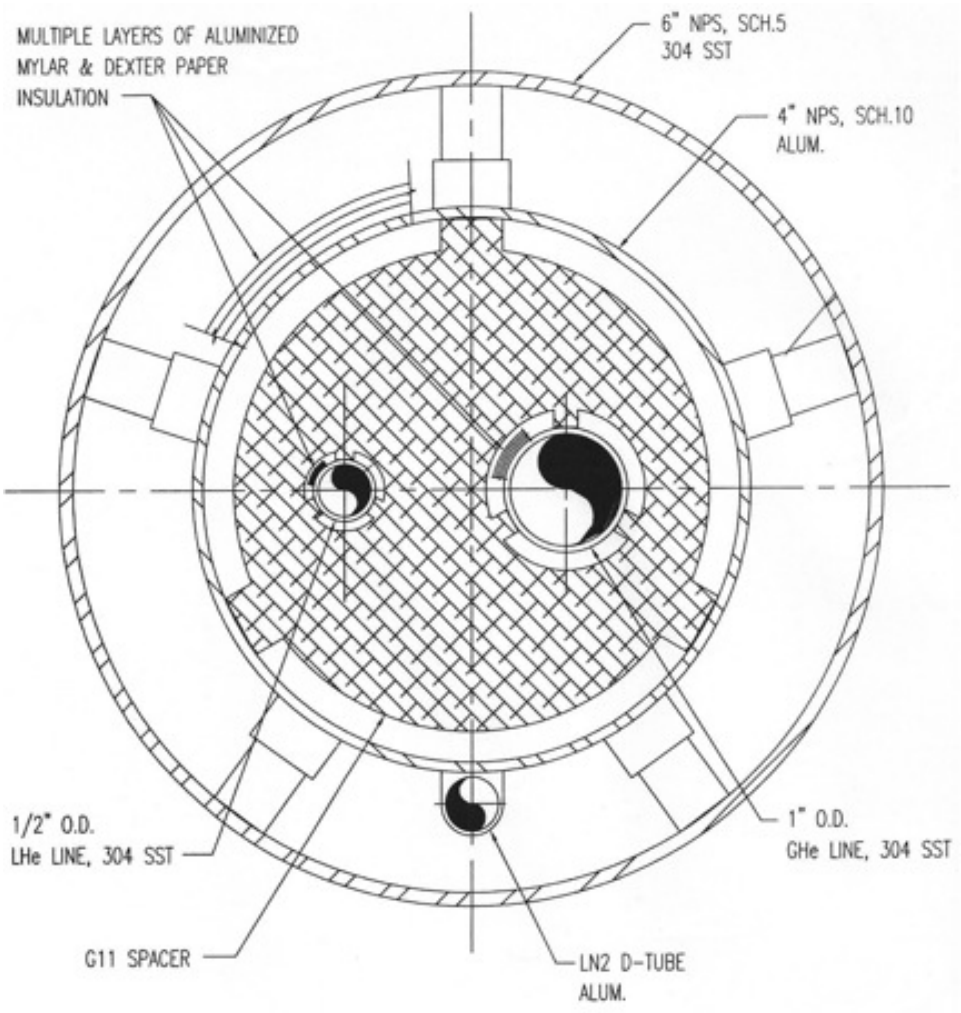

Figure 3: The cross-section of the VJ LHe line.

The cross-sectional geometry of the pipe is shown in Figure 3. The VJ line specifications as we move from the outside atmosphere towards the central axis are as follows:

Fitting No.	Fitting	Position along the pipe (m)	K	Position along the pipe (m)	K
		LHe line		GHe line - Cryostat return	
1	T-junction branch run	-	-	62.50	1.8
2	CRV	-	-	62.00	See Table 7
3	Pipe Entrance	0.00 (at Dewar)	1.0	-	-
4	90° Vertical Elbow	6.37	2.0	55.88	1.5
5	56° Elbow	13.76	0.5	48.49	0.38
6	55° Elbow	28.12	0.5	34.13	0.38
7	45° Vertical Elbow	34.46	0.4	27.79	0.3
8	45° Vertical Elbow	35.25	0.4	27.00	0.3
9	29° Elbow	38.12	0.2	24.13	0.15
10	45° Vertical Elbow	40.71	0.4	21.54	0.3
11	45° Vertical Elbow	41.65	0.4	20.60	0.3
12	15° Elbow	47.89	0.1	14.36	0.075
13	58° Vert./Hori. Elbow	52.61	0.5	9.64	0.38
14	22° Vertical Elbow	53.35	0.15	8.90	0.11
15	90° Vertical Elbow	55.70	2.0	6.55	1.5
16	Level Control Valve (LCV)	57.00	See (4)	-	-
17	90° Vertical Elbow	60.20	2.0	-	-
18	Pressure control Valve (PCV)	-	-	5.25	See Table 7
19	Venturi Meter	-	-	4.99	See (8)
20	Pipe Entrance	-	-	0.00	0.5

Table 3: Pipe fittings, their location along the length of the VJ line, and coefficients of frictional loss, K.

Fitting No.	Fitting	Position along the pipe (m)	K
		GHe line - Dewar return	
1	Pipe Entrance	0.00	0.5
2	90° Vertical Elbow	1.01	2.0
3	90° Vertical Elbow	2.51	2.0
4	90° Vertical Elbow	3.60	2.0
5	PCV	4.00	See Table 7
6	T-junction straight run	4.10	0.9
		GHe line - Heat exchanger	
7	Heat exchanger	-	See K_{eff}

Table 4: Pipe fittings, their location along the length of the GHe return lines, and coefficients of frictional loss, K.

- The outermost pipe is 6" NPS Schedule 5 304 Stainless Steel: OD = 6.625", ID = 6.407", Wall thickness = 0.109". The outer wall is assumed to be at $T = 294$ K (room temperature), and the inner wall is at $T_p = 77$ K (liquid nitrogen temperature).

- The inner pipe is cooled by liquid nitrogen at $T_p = 77$ K through conduction. The tube carrying the liquid nitrogen runs along the inner pipe in contact and every few meters spirals around the inner pipe.

- There is Multiple Layer Insulation (MLI) of Aluminized Mylar sheets interlaid with Dexter paper on the inner pipe. Each layer is 5×10^{-4} m thick and is assumed to have a linear temperature profile with thermal conductivity $k_{Al} = 0.07$ mW/(m K).

- The inner pipe is 4" NPS Schedule 10 Aluminum: OD = 4.5", ID = 4.26", Wall thickness = 0.120".

- There are G11 fibreglass epoxy spacers located throughtout the VJ line as shown in Table 5. Again these are the same spacers but, referenced with respect to different origins.

  The spacers maintain the LHe line and the GHe line that run inside the VJ line at a distance of 1" apart. The spacers reduce the heat conduction significantly by contacting the inner pipe, the LHe, and the GHe lines only at three points. With the inner side of the inner pipe, the total area of contact is only 4.95 cm^2. Effectively, this is the area across which heat transfer takes place, if any.

- Further, the model assumes that up to a radius of 6.5 cm from the central axis, the temperature is uniformly 4.5 K, the same as that of the LHe and GHe lines.

Spacer Number	Position along LHe line (m)	Position along GHe line (m)
1	4.49	57.21
2	6.17	55.53
3	7.03	54.67
4	7.23	54.47
5	7.44	54.26
6	10.10	51.60
7	12.77	48.93
8	13.96	47.74
9	15.14	46.56
10	17.12	44.58
11	17.32	44.38
12	19.99	41.71
13	22.66	39.04
14	25.32	36.38
15	27.99	33.71
16	28.32	33.38
17	29.76	31.94
18	30.62	31.08
19	33.29	28.41
20	34.84	26.86
21	37.03	24.67
22	39.08	22.62
23	39.94	21.76
24	41.17	20.53
25	43.43	18.27
26	46.09	15.61
27	49.26	12.44
28	50.53	11.17
29	52.91	8.79
30	53.48	8.22
31	55.49	6.21
32	55.90	5.80

Table 5: Distribution of spacers along the length of the VJ line.

- The LHe and GHe lines are wrapped in 20 layers of MLI.
- The LHe line is 0.5" OD 304 Stainless Steel pipe.
- The GHe line is 1.0" OD 304 Stainless Steel pipe.

Unlike the VJ line, the flexible hose connections at either end have no nitrogen shield. The number of layers of insulation used is also fewer (there are only 5); therefore heat loading in these sections of the transfer line are expected to be substantially higher than in the nitrogen-shielded section.

3 Two-Phase Flow Model

The model proposed in [6] is a one-dimensional homogeneous phase model for the two-phase liquid-gas flow in the transfer line. The model is one dimensional in that it ignores variation in properties in the radial and azimuthal directions. Accordingly, the thermodynamic properties are derived for a homogeneous mixture of gas and liquid. Further, it is assumed that the gas phase fraction (or void fraction, α) is less than 0.2, corresponding to bubbly flow throughout the length of the pipe. The flow is assumed to be turbulent, and therefore the flow is effective in mixing the gas and liquid phases. The model consists of conservation of gas mass, liquid mass, overall homogeneous phase momentum, and overall homogeneous phase energy balance equations [6].

In the present approach, the liquid transfer line is considered as one control volume. The fluid enters the control volume as saturated liquid ($\alpha_1 = 0$). The fluid is assumed to flash in the control volume. In the real LHe transfer line, the liquid flashes due to reduction in pressure due to line losses and due to heat transferred into the line through conduction and radiation. If the control volume is considered adiabatic, then reduction in pressure means the boiling point of the fluid is reduced. When the boiling point reaches the liquid temperature, the liquid flashes.

Given the inlet and outlet pressures and the void fraction of fluid entering the control volume, we are interested in estimating the void fraction at the exit (α_2) and the velocities at the inlet (v_1) and the outlet (v_2). The liquid-gas flow is assumed to be a homogeneous mixture with uniform velocities. To be able to solve for these three variables, we need three equations: mass conservation, momentum conservation, and energy conservation. In order to capture the dynamics associated with the opening and closing of the control valve and the pressure losses at each pipe fitting and line segment, the entire transfer line subdivided into multiple sections with end points placed where

process variables are to be evaluated. Details of the numerical methods and solution procedure are discussed in Section 7.

3.1 Mass balance for two-phase flow system

The mass balance equation for a control volume can be written as [1]:

$$\frac{\mathrm{d}m_{Tot}}{\mathrm{d}t} = \mathcal{F}_1 - \mathcal{F}_2 + r_{gen},$$

where m_{Tot} is the total mass in the control volume, $\mathcal{F}_1$ and $\mathcal{F}_2$ are the rates of mass flow into and out of the control volume (the entrance values are denoted with subscript 1 and the exit values with subscript 2), and r_{gen} is the rate of generation of mass. This equation can be split into mass balance equations for the two phases separately, taking into account the mass transferred between the phases,

$$\frac{\mathrm{d}m_g}{\mathrm{d}t} = \mathcal{F}_{g,1} - \mathcal{F}_{g,2} + r_{boil}$$

and

$$\frac{\mathrm{d}m_l}{\mathrm{d}t} = \mathcal{F}_{l,1} - \mathcal{F}_{l,2} - r_{boil},$$

where the subscript g denotes the gas phase and l denotes the liquid phase. The term r_{boil} denotes the rate at which mass is transferred from the liquid phase to the gas phase. This term can be further related to the rate of heat used in vaporization $\dot{Q}_{boil}$ and the latent heat of vaporization ζ as

$$r_{boil} = \frac{\dot{Q}_{boil}}{\zeta}.$$

However, when considering the overall mass balance on the control volume, there is no generation of mass inside the volume. At steady state, the conservation of total mass gives

$$0 = \mathcal{F}_1 - \mathcal{F}_2. \tag{1}$$

In terms of void fraction α, phase densities ρ_g and ρ_l, overall homogeneous velocities v, and cross-sectional areas A, this reduces to

$$\underbrace{(\rho_{g,1}\alpha_1 + \rho_{l,1}(1-\alpha_1))}_{\rho_1} A_1 v_1 = \underbrace{(\rho_{g,2}\alpha_2 + \rho_{l,2}(1-\alpha_2))}_{\rho_2} A_2 v_2, \tag{2}$$

where the density of the fluid at the entrance is ρ_1 given in terms of void fraction as $(\rho_{g,1}\alpha_1 + \rho_{l,1}(1-\alpha_1))$ and similarly the density at the exit of the control volume is ρ_2 given in terms of void fraction as $(\rho_{g,2}\alpha_2 + \rho_{l,2}(1-\alpha_2))$.

3.2 Momentum balance for two-phase flow system

The overall momentum balance in the control volume is [1]:

$$\begin{aligned}\frac{\mathrm{d}\mathbf{p}_{Tot}}{\mathrm{d}t} &= (P_1\mathbf{A}_1 - P_2\mathbf{A}_2) + m_{Tot}\mathbf{g} \\ &\quad - \mathbf{F}_f + \left(\rho_1\langle v_1^2\rangle\mathbf{A}_1 - \rho_2\langle v_2^2\rangle\mathbf{A}_2\right),\end{aligned}$$

where P_1 and P_2 are pressures on the inlet and outlet, $\mathbf{A}_1$ and $\mathbf{A}_2$ are the cross-sectional areas at the inlet and outlet, $\mathbf{g}$ is the acceleration due to gravity, and $\mathbf{F}_f$ represents the net force on the fluid due to solid boundaries. If the areas of inlet and outlet are equal ($A_1 = A_2 \equiv A = \frac{\pi}{4}d^2$), where d is the diameter of the pipeline and the normal is along the flow direction, then for a pipeline of uniform area of cross-section, the total mass in the control volume can be written as $\langle\rho\rangle AL$, where L is the length of the pipeline. The density $\langle\rho\rangle$ used here is the average density along the length of the line given by $(\rho_1 + \rho_2)/2$, where ρ_1 and ρ_2 are calculated from (2). The momentum balance for steady-state conditions, after dividing throughout by A, is

$$0 = (P_1 - P_2) + \langle\rho\rangle\,(Lg) - \sum_{i=1}^{n}\frac{1}{2}\langle\rho_i\rangle\langle v_i\rangle^2\left(\frac{L}{d}f_i + K_i\right) + \left(\rho_1 v_1^2 - \rho_2 v_2^2\right), \quad (3)$$

where Lg can be replaced with $g\Delta z$ accounting for change in elevation in the direction of gravity and n is the number of control volumes. For the ith control volume, the average density is $\langle\rho_i\rangle$ and the average velocity is $\langle v_i\rangle$. Evaluation of the frictional loss terms is done using average values in the control volume. The frictional loss due to a line length is given by $\left(\frac{L}{d}\right)f_i$ times the pressure head and due to a fitting is given by loss coefficient K_i (see Table 3) times the pressure head. The pressure head in any given control volume is given by $\frac{1}{2}\langle\rho_i\rangle\langle v_i\rangle^2$. The friction factor f_i corresponding to the ith line segment is evaluated using the Haaland expression [8] as:

$$f = \left\{-1.8\log_{10}\left[\frac{6.9}{Re_d} + \left(\frac{R_r}{3.7}\right)^{1.11}\right]\right\}^{-2},$$

where Re_d is the Reynolds number of the homogeneous flow based on diameter d of the pipe and $R_r = \epsilon/d$ is the relative roughness of the pipe. For steel pipes, the absolute roughness $\epsilon = 4.6 \times 10^{-5}$ m. For two-phase flow, the friction factor calculated from the above expression is corrected by a factor based on the void fraction of the flow given by $(1 + 0.5\alpha)$.

3.2.1 Control valve model

The level control valve is an equal-percentage-opening type valve with a loss coefficient of $K_{vs} = 5.0$ m^3/(h bar$^{1/2}$) when fully open. Assuming pure

liquid flow across the control valve, the pressure drop is given by

$$\Delta P_{\max} = \frac{\rho}{\rho_w}\left(\frac{\dot{V}_{\max}}{K_{vs}}\right)^2,$$

where ρ is density of fluid through the valve, ρ_w is density of water, and $\dot{V}_{\max}$ is the maximum volume flow rate through the valve for a calculated maximum pressure differential of ΔP_{max} in m^3/h. For an equal-percentage valve, the maximum flow rate is related to the volumetric flow rate at any fractional opening by [4]

$$\dot{V}_{\max} = \dot{V}\tau^{1-H},$$

where $\dot{V} = Av$ is the volumetric flow in the pipe, τ is the valve rangeability (typically $\sim$50), and H is fraction of valve opening. The control valve is handled separately, substituting the momentum balance equation with the pressure drop across the control valve to yield

$$\Delta P = \begin{cases} \frac{\rho}{\rho_w}\left(\frac{3600Av}{1.1\times H}\right)^2 & \text{if } H < 0.147, \\ \frac{\rho}{\rho_w}\left(\frac{3600\tau^{1-H}Av}{K_{vs}}\right)^2 & \text{if } H \geq 0.147. \end{cases} \tag{4}$$

3.3 Energy balance for two-phase flow system

The overall energy balance for the control volume is

$$\begin{aligned} \frac{\mathrm{d}E_{Tot}}{\mathrm{d}t} &= \rho_{g,1}\alpha_1 A_1 v_1\left(\mathcal{H}_{g,1} + \frac{1}{2}v_1^2 + gz_1\right) \\ &+ \rho_{l,1}(1-\alpha_1)A_1 v_1\left(\mathcal{H}_{l,1} + \frac{1}{2}v_1^2 + gz_1\right) \\ &- \rho_{g,2}\alpha_2 A_2 v_2\left(\mathcal{H}_{g,2} + \frac{1}{2}v_2^2 + gz_2\right) \\ &- \rho_{l,2}(1-\alpha_2)A_2 v_2\left(\mathcal{H}_{l,2} + \frac{1}{2}v_2^2 + gz_2\right) \\ &+ \dot{Q}_{ext} - \dot{W}, \end{aligned}$$

where E_{tot} is the total energy of the control volume, $\mathcal{H}$ denotes the enthalpy, $\dot{Q}_{ext}$ is the rate of heat transferred to the system, and $\dot{W}$ is the rate of work done by the system. For a steady-state model, the time derivative term on

the left-hand side vanishes, yielding

$$\begin{aligned}
0 = {} & \rho_{g,1}\alpha_1 A_1 v_1 \left(\mathcal{H}_{g,1} + \frac{1}{2}v_1^2 + g z_1\right) \\
& + \rho_{l,1}(1-\alpha_1) A_1 v_1 \left(\mathcal{H}_{l,1} + \frac{1}{2}v_1^2 + g z_1\right) \\
& - \rho_{g,2}\alpha_2 A_2 v_2 \left(\mathcal{H}_{g,2} + \frac{1}{2}v_2^2 + g z_2\right) \\
& - \rho_{l,2}(1-\alpha_2) A_2 v_2 \left(\mathcal{H}_{l,2} + \frac{1}{2}v_2^2 + g z_2\right) \\
& + \dot{Q}_{ext} - \dot{W}.
\end{aligned} \tag{5}$$

When there is no work done by the system, $\dot{W} = 0$. The external rate of heat transferred into the line ($\dot{Q}_{ext}$) is through radiation from the nitrogen-jacketed pipe enclosing the LHe line and GHe line. The lines are also insulated with MLI of Aluminized Mylar interleaved with Dexter paper. The Dexter paper reduces conduction, whereas the Aluminized Mylar surface shields the line from external radiation. The heat flux through the MLI is modeled by radiation and conduction fluxes; see Section 5.

3.3.1 Thermodynamic property model

The present model assumes two-phase flow and thermodynamic equilibrium between the gas and liquid phases. The pressure and temperature are then related to each other. The temperature can be estimated from the pressure along the saturation curve as [6]

$$T_{sat} = 0.232\, P^{\,0.252}, \tag{6}$$

which is a correlation based on NIST database [3] for saturated temperature T_{sat}, valid in the pressure range of $P = 0.6$–1.6 bar. The thermodynamic properties of the liquid and gas mixture are evaluated based on the void fraction. The liquid density ρ_l is taken constant, and the gas density is estimated based on the real gas law $\rho_g = \frac{P}{ZR_mT}$, where P, T, Z are the pressure, temperature, and compressibility of the gas at that point in the pipe and $R_m = R/M$ where $R = 8.314$ J/(mol K) is the universal gas constant and $M = 4.003$ g/mol is the molecular weight of helium. The overall mixture density in the cross-section is taken as $\rho = \rho_g\alpha + \rho_l(1-\alpha)$, and the viscosity is taken as $\mu = \mu_g\alpha + \mu_l(1-\alpha)$, where μ_g and μ_l are viscosity of the gaseous and liquid helium respectively. The variation in temperature in the system is only 0.3 K; therefore compressibility is evaluated as a function of pressure alone at $T = 4.5$ K:

$$Z = (8.222 \times 10^{-6} P + 0.4967)^{-1},$$

which is a correlation based on [3] for compressibility Z valid in the pressure range of $P = 1.0$–1.3 bar.

The internal energy as a function of pressure is obtained from the NIST database [3] as follows:

$$u = \lambda P^2 + \gamma P + \eta,$$

where the values of constants λ and γ for the correlation are taken from [6] and listed in Table 6.

	Liquid	Gas
λ	0.0	-1.9034×10^{-7}
γ	0.04897	0.03977
η	−5794.82	12638.58

Table 6: Correlation of internal energy u to pressure P from NIST database.

This correlation is valid in the pressure range of $P = 0.8$–1.9 bar. Further the enthalpy can be calculated as $h = u + P/\rho$, where h is the specific enthalpy in J/kg and u is specific internal energy in J/kg.

3.3.2 Work done by the system

In addition to the above equations, the amount of heat that goes into phase change can be found by

$$\dot{Q}_{boil} = \zeta \left(\rho_{g,2} \alpha_2 A_2 v_2 - \rho_{g,1} \alpha_1 A_1 v_1 \right),$$

where ζ is the heat of vaporization and the remaining expression is amount of gas formed equal to r_{boil}. Because the internal transfer of energy by latent heat of vaporization is not accounted for in the overall energy balance, it can be considered as the work done by the system for interface creation when the gas phase is formed. In fact, we show in Section 8.2 that it is essential to include this term in the place of rate of work done $\dot{W}$ to get good agreement with the measured data.

4 Gas-Phase Flow Model

For the GHe return line, there is no two-phase formation. The pressure and temperature are independent variables; however the void fraction is now known ($\alpha = 0$). Therefore, we still have three unknown variables, namely, pressure, temperature, and velocity or gas flow rate. The mass, momentum, and energy balances can be solved to calculate these variables.

4.1 Mass balance for gas-phase flow system

When considering the overall mass balance on the control volume, there is no generation of mass inside the volume. At steady state, the conservation of mass is given by (1). In terms of gas densities ρ_g, area of cross-section A, and homogeneous velocity v, the equation becomes

$$\rho_{g,1} A_1 v_1 = \rho_{g,2} A_2 v_2, \tag{7}$$

where the entrance values to the GHe return line are denoted with subscript 1 and the exit values with subscript 2.

4.2 Momentum balance for gas-phase flow system

The overall momentum balance in the control volume for steady-state conditions is given by (3). The gas pressures at the control volume inlet and outlet are denoted by P_1 and P_2. The densities are calculated based on equation of state for the pure gas flow. The GHe return line from the cryostat has a PCV, which is handled similar to the LCV on the LHe transfer line. The momentum balance equation for the control valve element is substituted by the pressure drop equation (4); see Section 3.2.1. The CRV of the GHe return from cryostat and the PCV on the dewar GHe return line are also handled similarly. The control valve parameters for the different control valves on the GHe network are given in Table 7.

Location	Loss coefficient for fully open valve (K_{vs})	Valve rangeability (τ)	Valve opening fraction (H)
PCV on GHe return from cryostat	5.0	50	Variable ($0 \rightarrow 1$)
CRV on GHe return from cryostat	5.8	75	1 (fully open)
PCV on GHe return from dewar	1.0	50	Variable ($0 \rightarrow 1$)

Table 7: Control valve parameters.

In addition to the control valves, there is a venturi flow meter on the GHe return line from cryostat that causes a pressure drop. The mass flow rate measured by the venturi meter is correlated to the pressure drop across the meter as follows:

$$\mathcal{F}_v = 0.0481 \Delta P^{\,0.50483}, \tag{8}$$

where the mass flow rate $\mathcal{F}_v$ is given in kg/s and pressure drop ΔP is measured in bars.

4.3 Energy balance for gas-phase flow system

The overall energy balance for the control volume at steady state is given by

$$0 = \rho_{g,1} A_1 v_1 \left(\mathcal{H}_{g,1} + \frac{1}{2} v_1^2 + g z_1 \right) - \rho_{g,2} A_2 v_2 \left(\mathcal{H}_{g,2} + \frac{1}{2} v_2^2 + g z_2 \right) + \dot{Q}_{ext}. \tag{9}$$

The rate of heat transferred into the GHe return line $\dot{Q}_{ext}$ comes from heat loading on the VJ line or the flexible hose connections, discussed further in Section 5. The Soave–Redlich–Kwong equation of state is used for modeling the pressure-volume-temperature relationship. If convergence of the iterations used to solve the equation of state is not achieved, the previously noted NIST database correlations (see Section 3.3.1) are used.

5 The Heat Network

The external heat transferred into the LHe line and GHe line is denoted by $\dot{Q}_{ext}$ in equations (5) and (9), respectively. To calculate the total heat load on the LHe line, the following heat transmissions are considered:

- The total rate of heat transfer from the inner surface of the inner pipe (denoted by subscript p) to the first layer of the MLI on the LHe pipe (denoted by subscript 0) by radiation, $\dot{Q}^R_{p,0}$.
- The rate of heat transfer from successive layers of the MLI to the outer surface of the pipe by radiation, $\dot{Q}^R_{m,m+1}$ where m denotes the mth MLI layer amongst n layers; $m : 0 \rightarrow N$. In the present case, $N = 20$ for LHe and GHe lines inside the VJ line and $N = 5$ for flexible hoses used on both LHe and GHe lines.
- The rate of heat transfer through the MLI by conduction, $\dot{Q}^C_{m,m+1}$.

The rate at which heat is transferred from the inner pipe to the insulation layers is then transferred across the insulation layers by conduction and radiation. The same is true for flexible hose lines; however there is no nitrogen shield. Therefore, for hose lines, the inner pipe is at room temperature (294 K) instead of the temperature of liquid nitrogen (77 K).

The total rate of heat transfer can be written as

$$\dot{Q}^R_{p,0} = \dot{Q}^R_{m,m+1} + \dot{Q}^C_{m,m+1}. \tag{10}$$

5.1 Heat transfer by radiation

In general, the rate of heat transfer by radiation from any surface m to another parallel surface $m+1$ is given by:

$$\dot{Q}^R_{m,m+1} = \frac{\sigma(T_m^4 - T_{m+1}^4)}{R_{m,m+1}}, \tag{11}$$

where $\dot{Q}^R_{m,m+1}$ is the rate of radiative heat transfer (in W), σ is the Stefan–Boltzmann constant (5.678×10^{-8} W/(m^2 K^4)), T_m and T_{m+1} are the temperatures of surfaces m and $m+1$ respectively (in K), and $R_{m,m+1}$ is the surface radiative resistance between surfaces m and $m+1$ (in m^{-2})

The radiative resistance $R_{m,m+1}$, is calculated as follows [2]:

$$R_{m,m+1} = \left[\frac{1-\epsilon_m}{\epsilon_m A_m} + \frac{1}{A_m F_{m,m+1}} + \frac{1-\epsilon_{m+1}}{\epsilon_{m+1} A_{m+1}}\right],$$

where m and $m+1$ are surfaces that send and receive radiation, with areas A_m and A_{m+1}, and $F_{m,m+1}$ represents the view factor of surface $m+1$ from surface m. The emissivities of the surfaces are given by ϵ_m and ϵ_{m+1}, respectively. The calculation of the view factor considers the following criteria:

- For radiation transfer through insulation layers, the view factor for an outer layer of insulation to an immediate inner layer is 1. However, there is an area difference due to layer thickness.
- For radiation transfer through vaccuum, the view factor for the inner surface of the inner pipe to the outer layer of insulation on either LHe or GHe line is less than 1. This is because only part of the radiation is received by the LHe line and the GHe line. The remaining radiation is received by the inner surface of the pipe itself; see Figure 3. Due to this complication, the view factor is computed indirectly. The view factor from the LHe line is calculated and adjusted for areas as follows:
  - The view factor from one pipe to another pipe (in the present case from LHe line to the GHe line) is given by:

$$\begin{aligned} F_{LHe,GHe} = \frac{1}{2\pi}\Bigg[\pi &+ \left(C^2 - (r+1)^2\right)^{1/2} - \left(C^2 - (r-1)^2\right)^{1/2} \\ &+ (r-1)\cos^{-1}\left(\frac{r}{C} - \frac{1}{C}\right) \\ &- (r+1)\cos^{-1}\left(\frac{r}{C} + \frac{1}{C}\right)\Bigg], \end{aligned}$$

where $r = \frac{r_{GHe}}{r_{LHe}}$, r_{GHe} and r_{LHe} are the radii of GHe and LHe lines including insulation, and $C = 1 + r + \frac{s}{r_{LHe}}$, where s is the closest distance between GHe and LHe lines. The view factor from outer layer of the MLI of the LHe line (denoted by $m = 0$) to the pipe surface (denoted by subscript p) is

$$F_{0,p} = 1 - F_{LHe,GHe}.$$

This means that the view from LHe line to the inner surface of the pipe is the total view minus the view obstructed by the presence of GHe line.

– Adjusting for the areas receiving and transmitting heat, we express the reverse view factor as

$$F_{p,0} = \frac{A_0}{A_p} F_{0,p}.$$

A similar procedure is followed for the GHe line. The emissivity of the Aluminized Mylar layer may change due to the temperature profile across the insulation; it is calculated as

$$\epsilon_{Al} = 0.012 + 4.044 \times 10^{-5}(T - 4). \tag{12}$$

5.2 Heat transfer by conduction through the MLI

Consider the heat transfer by conduction from an outer layer m to the next inner layer $m + 1$, given by

$$\dot{Q}^C_{m,m+1} = -k_{Al} A_m \left(\frac{T_{m+1} - T_m}{r_{m,m+1}} \right),$$

where, $\dot{Q}^C_{m,m+1}$ is the heat transfer rate by conduction in W, k_{Al} is the thermal conductivity of collective insulation (one insulation layer consists of a Aluminized Mylar film insulated from next film by a layer of Dexter paper) in W/(m K), A_m is the area through which heat is conducted in m^2, and T_m and T_{m+1} are the temperatures of layers m and $m+1$ of insulation in K. Let T_0 be the temperature of the outermost layer and T_N be the temperature of the innermost layer, both in K. According to this notation, T_{N+1} is then equal to the temperature of the line T_{LHe}. The effective thickness of the cylindrical layers is given by $r_{m,m+1} = r_m \ln(\frac{r_m}{r_{m+1}})$, in m.

When the expressions for heat transfer by conduction and radiation are

substituted into the overall heat transfer rate equation, we obtain

$$\begin{aligned}\frac{\sigma(T_p^4 - T_0^4)}{R_{p,0}} &= \frac{\sigma(T_0^4 - T_1^4)}{R_{0,1}} + k_{Al}A_0\frac{T_0 - T_1}{r_{0,1}} \\ &= \frac{\sigma(T_m^4 - T_{m+1}^4)}{R_{m,m+1}} + k_{Al}A_m\frac{T_m - T_{m+1}}{r_{m,m+1}} \\ &= \frac{\sigma(T_N^4 - T_{LHe}^4)}{R_{N,LHe}} + k_{Al}A_N\frac{T_N - T_{LHe}}{r_{N,LHe}}. \end{aligned} \tag{13}$$

The temperature of the inner surface of the inner pipe is $T_p = 77$ K, i.e., the temperature of liquid nitrogen. The temperature of the LHe pipe is $T_{LHe} = 4.5$ K. Equation (13) can be solved for the temperature of the outer layer of insulation T_0 using a non-linear solver. The emissivity of the MLI (ϵ_{Al}) is a function of temperature (12) unless T_0 is less than 6 K. Otherwise, an initial value of $\epsilon_{Al} = 0.012$ is assumed in the expression for $R_{m,m+1}$. We solve for T_0, assume a linear profile in the MLI, calculate ϵ_{Al}, and iterate until $\delta T_0 < 0.1$ K. The emissivity of the aluminum pipe used for the inner pipe is 0.09 (the value for commercial sheet aluminum). The emissivity of the braided steel pipe is taken as 0.23 (the value for new galvanized steel). These values are taken from [7].

5.3 Heat transfer by conduction through spacers

The heat transfer by conduction is given by

$$\dot{Q}_{G11}^{C} = -k_e A\left(\frac{T_{LHe} - T_p}{\Delta x_s}\right), \tag{14}$$

where k_e is the thermal conductivity of the fiberglass epoxy in W/(m K), A is the area of heat transfer, and Δx_s is the distance from the inner pipe surface to the 6.5 cm circle in the epoxy spacer. The LHe and GHe lines are placed 1" apart. All the heat flux is through the three contact points of the spacer and the inner pipe; hence the area of heat transfer is taken as $A = 1.27$ cm $\times 1.30$ cm $\times 3 = 4.95$ cm^2. Assuming all the heat is absorbed by the LHe line and the GHe line, the fraction that goes into the LHe line is proportional to the surface area of LHe line to GHe line.

6 The Cryostat Model

The dynamic model of the cryostat is based on the differential equations describing change of gas mass, liquid mass, volume of liquid, and pressure

inside the cryostat, as derived in [5]. The final equations used in the present simulation are reproduced here for convenience:

$$\frac{\mathrm{d}m_l}{\mathrm{d}t} = \mathcal{F}_{l,1} - \mathcal{F}_{l,2} - r_{boil}, \tag{15}$$

$$\frac{\mathrm{d}P_c}{\mathrm{d}t} = \frac{a_1}{a_2} + r_{boil}\left(\frac{u_l - u_g}{a_2}\right), \tag{16}$$

where r_{boil} is the rate of boiling of LHe in the cryostat, given by

$$r_{boil} = \frac{-\frac{a_1}{a_2}\left(a_3 + 0.0585 a_4 m_l \phi P_c^{-0.748}\right) + a_4\left[\frac{V_g}{m_g}\left(\mathcal{F}_{g,2} - \mathcal{F}_{g,1}\right) + a_5\left(\mathcal{F}_{l,2} - \mathcal{F}_{l,1}\right)\right]}{\frac{u_l - u_g}{a_2}\left(a_3 + 0.0585 a_4 m_l \phi P_c^{-0.748}\right) + a_4\left(\frac{V_g}{m_g} - a_5\right)},$$

where,

$$\begin{aligned}
a_1 &= \dot{Q}_{cryo} + \mathcal{F}_{l,1}\left(h_{l,1} - u_{l,1}\right) + \mathcal{F}_{g,1}\left(h_{g,1} - u_{g,1}\right) \\
&\quad - \mathcal{F}_{l,2}\left(h_{l,2} - u_{l,2}\right) - \mathcal{F}_{g,2}\left(h_{g,2} - u_{g,2}\right) \\
a_2 &= 0.0585\left(m_l C_{v,l} + m_g C_{v,g}\right) P_c^{-0.748} \\
a_3 &= 0.0585 P_c^{-0.748} - \frac{\left(16.444 \times 10^{-6} P_c + 0.4967\right) V_g}{R m_g} \\
a_4 &= \frac{\left(8.222 \times 10^{-6} P_c^2 + 0.4967 P_c\right)}{R m_g} \\
a_5 &= 0.232 \phi P_c^{0.252} + \psi,
\end{aligned}$$

where P_c is the pressure inside the cryostat, m_l and m_g are the masses of liquid and gaseous helium, V_l and V_g are the volumes of liquid and gaseous helium, $\mathcal{F}_{l,1}$ and $\mathcal{F}_{l,2}$ are the mass flow rates of liquid helium into and out of the cryostat, and $\mathcal{F}_{g,1}$ and $\mathcal{F}_{g,2}$ are the mass flow rates of GHe into and out of the cryostat, respectively. The specific enthalpy and internal energy of the streams are represented by h and u with corresponding subscripts. The gas exiting the cryostat is assumed to have the same thermodynamic properties as the gas in the crysotat. The internal energy and enthalpy for LHe and GHe are calculated based on the NIST database correlations presented in Table 6. The constants $\phi = 0.0017612$ and $\psi = 0.0004873$ for the linear correlation of the specific volume (a_5) are based on the NIST database [6] as a function of temperature. The cryostat is assumed to be operating in thermal equilibrium at all times; therefore the temperature is dependent on pressure according to equation (6). The constant volume heat capacities are $C_{v,l} = 2584$ J/(kg K) and $C_{v,g} = 3201$ J/(kg K) for liquid and gas, respectively. The rate of heat input into the cryostat is $\dot{Q}_{cryo}$, consisting of three portions, namely, the heat input from RF Cavity ($\dot{Q}_{RF}$), the heating resistor ($\dot{Q}_H$), and the static heat loading from the surroundings ($\dot{Q}_s$); see next section.

6.1 Static heat loading model

In order to model the static loading, the cryostat is operated at various heater inputs with the RF Cavity in maintenance mode; i.e., there is no heat input from the RF Cavity ($\dot{Q}_{RF} = 0$). For any given setting of heater power input, the valve positions of the LCV on the LHe transfer line and the PCV on the GHe return line are noted for steady-state operation. The mass flow rates of LHe and GHe from the LHe transfer line and the mass flow rate of GHe helium out of the cryostat into the GHe return line and the constant gas flow stream drawn for waveguide cooling are estimated. Based on these estimates, the amount of GHe formed in the cryostat can be estimated. The total heat power into the cryostat due to static loading and heater power input must be balanced by the amount of latent heat used in the phase change of the helium. Because the amount of heat used in phase change can be estimated based on amount of GHe formed, the static heat loading can be correlated to the heater power input. The following static heat loading correlation is arrived at based on various measured values of heater power inputs:

$$\dot{Q}_s = -0.27874\dot{Q}_H + 54.754. \tag{17}$$

6.2 Controller model

The normal pressure in the cryostat is to be maintained within ±1 mbar for consistent operation of the RF Cavity. Both the level of the LHe and pressure of the GHe are regulated by proportional-integral controllers. The control valve lift is calculated as

$$H(i) = K_p \left(\epsilon(i) + \frac{1}{T_I} \sum_{i=1}^{n_{steps}} \epsilon(i)\Delta t \right), \tag{18}$$

where the error is calculated as $\epsilon(i)$ = (Set value – Measured value) for mode-1 operation (positive mode) and $\epsilon(i)$ = (Measured value – Set value) for mode-2 operation (negative mode). The variable i represents any time level, and for the integral controller, the summation is from the start of operation ($i = 1$) to current time level ($i = n_{steps}$) after n_{steps} time steps of size Δt. K_p is proportional gain of the controller and T_I is the time constant for integral controller. The level controller operates in mode-1 and the pressure controller operates in mode-2. The controller settings normally used are given in Table 8.

Controller	Set Value	K_p	T_I
LCV on LHe	70-75%	10%/%	100
PCV on GHe	1.22 bars	20%/bar	50
FCV on waveguide stream	25 L/min	2%/(L/min)	10

Table 8: Controller parameters.

7 The Numerical Methods

In the following section, we present the implementation details of the control-volume approach for simulating the LHe transfer line and the GHe return line.

7.1 Control-volume definition

The results of lumped system simulation of the LHe transfer line and GHe return network presented in Section 8 are based on the points tabulated in Table 9 for the LHe transfer line, Table 10 for the GHe return line from cryostat, and Table 11 for the GHe return line from the dewar. The line segment from the T-junction to the compressor suction is assumed to be of unit length with only two end points, i.e., the T-junction outlet and the compressor suction inlet. The equations for mass balance (2), momentum balance (3), and energy balance (5) are solved for each of the control volumes defined between any two points using the `fsolve` routine in MATLAB^{TM}.

In the tables, the first column is the point number; the second is the location of the point along the length of the transfer line. It is possible for two successive points to be at the same location, implying that the element in between is a pipe fitting or valve, which is assumed to have zero line length but has a loss coefficient. In such cases, the entry in fourth column for length of line segment is zero and the entry in sixth column for loss coefficient K_i is non-zero. The opposite is true for a finite-length line segment. A special case is the control valve, for which the loss coefficient is indicated as -1 to enable the program to identify the element as a control valve. The venturi meter on the GHe return from the cryostat is indicated as -2 to distinguish it for the program, and -3 is used for cold return valve. The third column is the elevation of the control volume with respect to the datum $z = 0.0$ set at the pipe inlet at the dewar. The same datum is used for the entire pipeline. The fifth column is the diameter of the line segment. A constant diameter is assumed for all fittings, valves, and connecting pipes. The last column is the external heat input into the control volume.

Point no.	Location along the pipe (in m)	Elevation (in m)	Length of line segment (in m)	Diameter of line (in m)	Loss Coefficient (K_i)	External heat input Q_i (in W)
1	0	0	0	0.009398	0	0
2	0	0	0	0.009398	1	0
3	1.75	1.75	1.75	0.009398	0	0
4	4.29	3.02	2.54	0.009398	0	0.78926
5	6.37	5.1	2.08	0.009398	0	0.067819
6	6.37	5.1	0	0.009398	2	0
7	13.76	5.1	7.39	0.009398	0	0.17483
8	13.76	5.1	0	0.009398	0.5	0
9	28.12	5.1	14.36	0.009398	0	0.28585
10	28.12	5.1	0	0.009398	0.5	0
11	34.46	5.1	6.34	0.009398	0	0.1409
12	34.46	5.1	0	0.009398	0.4	0
13	35.25	4.54	0.79	0.009398	0	0.033306
14	35.25	4.54	0	0.009398	0.4	0
15	38.12	4.54	2.87	0.009398	0	0.038326
16	38.12	4.54	0	0.009398	0.2	0
17	40.71	4.54	2.59	0.009398	0	0.06905
18	40.71	4.54	0	0.009398	0.4	0
19	41.65	5.2	0.94	0.009398	0	0.033668
20	41.65	5.2	0	0.009398	0.4	0
21	47.89	5.2	6.24	0.009398	0	0.077858
22	47.89	5.2	0	0.009398	0.1	0
23	52.61	5.2	4.72	0.009398	0	0.07419
24	52.61	5.2	0	0.009398	0.5	0
25	53.35	5.48	0.74	0.009398	0	0.033186
26	53.35	5.48	0	0.009398	0.15	0
27	55.7	5.48	2.35	0.009398	0	0.068471
28	55.7	5.48	0	0.009398	2	0
29	56.39	4.78	0.69	0.009398	0	0.001665
30	57	4.78	0.61	0.009398	0	0
31	57	4.78	0	0.009398	-1	0.59
32	57.6	3.57	0.6	0.009398	0	0
33	60.2	2.255	2.6	0.009398	0	1.1191
34	60.2	2.255	0	0.009398	2	0
35	60.3	2.155	0.1	0.009398	0	0

Table 9: Points chosen for the LHe transfer line simulation.

Point no.	Location along the pipe (in m)	Elevation (in m)	Length of line segment (in m)	Diameter of line (in m)	Loss Coefficient (K_i)	External heat input Q_i (in W)
1	0	2.465	0	0.022911	0	0
2	0	2.465	0	0.022911	0.5	0
3	2.63	3.78	2.63	0.022911	0	1.4488
4	3.38	4.53	0.75	0.022911	0	0
5	4.99	4.53	1.61	0.022911	0	0
6	4.99	4.53	0	0.022911	−2	0
7	5.25	4.53	0.26	0.022911	0	0
8	5.25	4.53	0	0.022911	−1	0.59
9	6.35	5.28	1.1	0.022911	0	0.12923
10	6.55	5.48	0.2	0.022911	0	0.00065944
11	6.55	5.48	0	0.022911	1.5	0
12	8.9	5.48	2.35	0.022911	0	0.13335
13	8.9	5.48	0	0.022911	0.11	0
14	9.64	5.2	0.74	0.022911	0	0.0024399
15	9.64	5.2	0	0.022911	0.38	0
16	14.36	5.2	4.72	0.022911	0	0.14116
17	14.36	5.2	0	0.022911	0.075	0
18	20.6	5.2	6.24	0.022911	0	0.20897
19	20.6	5.2	0	0.022911	0.3	0
20	21.54	4.54	0.94	0.022911	0	0.0030994
21	21.54	4.54	0	0.022911	0.3	0
22	24.13	4.54	2.59	0.022911	0	0.13414
23	24.13	4.54	0	0.022911	0.15	0
24	27	4.54	2.87	0.022911	0	0.13506
25	27	4.54	0	0.022911	0.3	0
26	27.79	5.1	0.79	0.022911	0	0.0026048
27	27.79	5.1	0	0.022911	0.3	0
28	34.13	5.1	6.34	0.022911	0	0.3349
29	34.13	5.1	0	0.022911	0.38	0
30	48.49	5.1	14.36	0.022911	0	0.48695
31	48.49	5.1	0	0.022911	0.38	0
32	55.88	5.1	7.39	0.022911	0	0.40117
33	55.88	5.1	0	0.022911	1.5	0
34	57.96	3.02	2.08	0.022911	0	0
35	61.5	1.25	3.54	0.022911	0	1.529
36	62	1.25	0.5	0.022911	0	0
37	62	1.25	0	0.022911	−3	0.47
38	62.5	1.25	0.5	0.022911	0	0
39	62.5	1.25	0	0.022911	1.8	0

Table 10: Points chosen for simulation of GHe return line from the cryostat.

Point no.	Location along the pipe (in m)	Elevation (in m)	Length of line segment (in m)	Diameter of line (in m)	Loss Coefficient (K_i)	External heat input Q_i (in W)
1	0	0	0	0.015799	0	0
2	0	0	0	0.015799	0.5	0
3	1.01	1.01	1.01	0.015799	0	0.27577
4	1.01	1.01	0	0.015799	2	0
5	2.51	1.01	1.5	0.015799	0	0.40956
6	2.51	1.01	0	0.015799	2	0
7	3.6	−0.08	1.09	0.015799	0	0.29762
8	3.6	−0.08	0	0.015799	2	0
9	4	−0.08	0.4	0.015799	0	0.10922
10	4	−0.08	0	0.015799	−1	0.47
11	4.1	−0.08	0.1	0.015799	0	0.027304
12	4.1	−0.08	0	0.015799	0.9	0

Table 11: Points chosen for simulation of GHe return line from the dewar.

7.2 The LHe transfer line solution

For the LHe transfer line, the three variables at any point are the pressure, velocity, and void fraction. By assuming saturated fluid conditions throughout the pipeline, we can eliminate temperature as a degree of freedom. For the first control volume, the inlet void fraction of the fluid stream is assumed zero; i.e., the liquid is saturated. The pressure at the inlet of the pipe is known; it is equal to dewar operating pressure. We then need to estimate the velocities at the inlet and outlet as well the void fraction at the outlet. The pressure at the outlet of the first control volume is not known. However, the outlet pressure of the final control volume is known; it is equal to the cryostat pressure. If there are n control volumes, we can write $3n$ equations. At the first point, there is 1 unknown, at the last point there are 2 unknowns, and at all $n-1$ intermediate points, there are 3 unknowns, thus adding up to $3n$ variables. In other words, there is sufficient number of equations for closure, and in principle the entire system can be solved.

The boundary conditions and the corresponding thermodynamic properties for LHe transfer line are known or estimated [3] as in Table 12.

7.3 The GHe network solution procedure

The GHe network has three segments and the T-junction. There are three terminals, namely, the cryostat, the dewar, and the compressor suction.

Property	Inlet (1)	Outlet (2)
Pressure (P, in bars)	1.37	1.22
Temperature ($T = T_{sat}$, in K)	4.5682	4.4345
Height (z, in m)	0.0	0.105
Diameter (d, in m)	0.009398	0.009398
Liquid		
Enthalpy (H_l, in J/kg)	2037.2	1173.6
Internal Energy (U_l, in J/kg)	866.94	160.13
Density (ρ_l, in kg/m^3	117.06	120.38
Gas		
Enthalpy (H_g, in J/kg)	20394	20619
Internal Energy (U_g, in J/kg)	14509	14640
Density (ρ_g, in kg/m^3)	23.278	20.407

Table 12: Boundary conditions for simulation and corresponding thermodynamic properties.

The pressure and temperature conditions at these end points are known. However, the mass flow rate in any of these segments is dependent on the valve openings. The solution method proceeds in the following steps:

- For the GHe return line from the cryostat, the pressure and temperature at the entrance, i.e., the exit of cryostat, are known; they are taken to be the same as the cryostat pressure ($P_1 = P_c$) and temperature ($T_1 = T_c$). The pressure (P_T) and temperature (T_T) at T-junction or the velocities v_1 and v_2 at either ends are unknown. Thus, there are four variables. However, there are only three equations, viz., mass balance (7), momentum balance (3), and energy balance (9). The following scheme is used starting with an initial guess of mass flow rate from cryostat $\mathcal{F}_c$ for any given pressure control-valve opening.

- Using the pressure at the T-junction (P_T) calculated above, the GHe return line from dewar can be solved fully for the velocities and temperature at the T-junction using the same set of equations, viz., mass balance (7), momentum balance (3), and energy balance (9). The temperatures and velocities of GHe return streams from cryostat and dewar are generally different. Let $T_{T,d}$ be the temperature of the stream from the dewar, $T_{T,c}$ be the temperature of the stream from the cryostat, $\mathcal{F}_d$ be mass flow rate from the dewar, and $\mathcal{F}_c$ be the mass flow rate from the cryostat.

- The mass balance gives the total mass flow rate to the compressors:

$$\mathcal{F}_{Tot} = \mathcal{F}_d + \mathcal{F}_c.$$

However, the total mass flow rate is not accurate until convergence is achieved.

- The energy balance at the T-junction gives the temperature of the mixed stream as follows:

$$T_T = (\mathcal{F}_c T_{T,c} + \mathcal{F}_d T_{T,d})/(\mathcal{F}_{Tot}).$$

- The pressure (P_{cp}) and temperature (T_{cp}) at the compressor suction are known. Provided the loss coefficient across the heat exchanger network (K_{eff}) is available, the velocity at the compressor suction can be calculated using the momentum balance equation (3). This value can then be used for updating the mass flow rate ($\mathcal{F}_c$) in the GHe return stream from cryostat.

In order to estimate an average value of the effective loss coefficient across the heat exchanger, the above calculations are performed with known values of gas mass flow rates from cryostat measured by the venturi meter (8). A sample of the measured data is given in Table 15. The PCV on the dewar is assumed to be open 80% at all times, and the CRV is assumed to be fully open. A K_{eff} value of approximately 54 is obtained. This effective loss coefficient K_{eff} is used for subsequent simulations where the mass flow rate from cryostat is unknown. This is the case in the following dynamic simulation, where the cryostat valve is dynamically operated based on the pressure in the cryostat.

7.4 Dynamic simulation of the cryostat

The cryostat model is a dynamic model based on ordinary differential equations of the form $\frac{\mathrm{d}y}{\mathrm{d}t} = f(t, y)$ that are discretized in time by the first-order explicit forward Euler scheme,

$$\frac{y_i - y_{i-1}}{\mathrm{dt}} = f(t_{i-1}, y_{i-1}), \tag{19}$$

by the first-order implicit backward Euler scheme,

$$\frac{y_i - y_{i-1}}{\mathrm{dt}} = f(t_i, y_i), \tag{20}$$

or by the second-order implicit Crank–Nicolson scheme

$$\frac{y_i - y_{i-1}}{\mathrm{dt}} = \frac{1}{2}\left(f(t_i, y_i) + f(t_{i-1}, y_{i-1})\right). \tag{21}$$

The time step size has been denoted by dt for future reference. The time step dt is assumed to be sufficiently small but not infinitesimal. In our simulations, we have taken $\mathrm{dt} = \Delta t$ from(18), but this is not required.

In order to simulate the cryostat dynamics, the following iteration for any time level i is followed:

- Given the pressure in the cryostat and the dewar at time level i, the LHe transfer line is solved for liquid and gas flow rates into the cryostat using equations (2), (3), and (5).
- Given the pressures in the cryostat, the dewar, and at the compressor suction at time level i, the GHe return network is solved for the gas flow rate out of the cryostat following the procedure in Section 7.3. Note that a small constant stream of gas is drawn to cool the waveguide attached to the cryostat.
- Using the flow rates of liquid and gas into and out of the cryostat along with the heater power input, the change in mass of LHe inside the cryostat (15) and hence the volume of helium and the level of LHe can be estimated. Using the differential equation for pressure (16), the cryostat pressure for the next time step $i + 1$ can be determined.
- The updated pressure and level in the cryostat at time level $i + 1$ are used for calculating the error terms $\epsilon(i)$ at any time level i in equation (18). The pressure controller on the cryostat is mode-2 operation; i.e. if the pressure is higher than the set pressure, the error is positive and the PCV valve must open to relieve some of the gas in the cryostat. The level controller on the cryostat is in mode-1 operation; i.e. if the level is lower than the set level, the error is positive and LCV must open to allow flow into the cryostat. After the correction, the valve position at the time level $i + 1$ is known.
- Using the updated valve positions and pressure in the cryostat, the procedure can be repeated for the next time step.

The flow rates in the above iteration scheme are determined based on current time level (i) values of pressure, hence making it an explicit method. For the implicit method, the flows rates are updated based on the predicted pressure in the cryostat, and these updated flow rates are then used to correct the pressure and the level in the cryostat before making changes to the valve positions in the pressure and level control valves. Alternatively, the values of flow rates obtained at current and predicted values of pressure could be weighted equally to obtain a corrected pressure and level in the cryostat that can then be used for updating the valve positions. This leads to the second-order implicit method known as the Crank–Nicolson scheme.

8 Results

In this section, we present the validation of liquid flow rate and gas flow rate from the LHe transfer line into the cryostat. This is a critical test for the accuracy of the code developed. The second validation case presented is the dynamic operation of the cryostat along with the controllers in response to heater power step input changes. This test assesses the accuracy of not only the LHe transfer line calculations but also the GHe return network along with the cryostat and controller models. The dynamic one-dimensional homogeneous model from [6] is used for a comparison of the results.

8.1 External heat transfer

The rate of heat transfer by conduction and radiation according to the heat network equation (13) is evaluated using non-linear solver `fsolve` in MATLAB. The output from the program is tabulated in Table 13 for the LHe transfer line and the GHe return network.

Presently the program uses 5 layers of Aluminized Mylar Insulation on LHe line inside the flexible line from the dewar to the VJ line and the flexible line from the VJ line to the cryostat. The same number of layers is assumed for other flexible lines. The LHe line and GHe line inside the VJ line have 20 layers each.

In addition to the heat transferred by radiation from the jacket pipe and conduction through the MLI, we also have conduction from the jacket pipe by conduction through the spacer material. The estimate of this rate of heat transferred is given in [6] as 1.005 W into the LHe transfer line and 2.01 W into the GHe return line from the cryostat. The heat transferred through the spacers is distributed among the 32 spacers and is applied as such.

The control valve stem is also a source of heat load into the LHe line and is estimated to be 0.59 W for the LCV. The same value is used for the PCV on the GHe return line from the cryostat, and the CRV puts in an additional 0.47 W into this line. The heat loading through the valve stem of the PCV on the GHe return from the dewar is 0.47 W. The heat input through the control valve is used when solving for the control volume encompassing the control valve.

The total heat loading on the LHe transfer line is estimated as 3.59 W, on the GHe return line from the cryostat as 6.15 W, and on the GHe return line from the dewar as 1.59 W.

Line Section	MLI Outer Layer Temperature	MLI Outer Layer Emissivity	Radiative Resistance ($1/m^2$)	Rate of external heat transferred per unit length (W/m)	Rate of external heat input in section (W)
LHe transfer line					
Dewar Flex Line:	228.4	0.0211	341.69	0.31073	0.789
Main VJ Line - LHe:	9.7	0.0122	16.00	0.00241	0.125
Cryostat Flex Line:	223.0	0.0209	250.69	0.43041	1.132
GHe return line					
Cryostat flex line:	220.5	0.0208	200.23	0.55087	1.449
Main VJ Line - GHe:	8.9	0.0122	11.71	0.00330	0.170
Coldbox Flex Line:	223.7	0.0209	184.48	0.43192	1.529
Dewar Return Line:	279.6	0.0231	68.87	0.27304	1.119

Table 13: The rate of external heat transferred into various sections by radiation and conduction through MLI surface.

8.2 The liquid flow rate

The liquid flow rate calculated using the program is plotted for various control valve lift positions denoted by H, which takes a value of 0.0 for fully closed to 1.0 for fully open. Figure 4 compares the present program output to that of the one-dimensional homogeneous model.

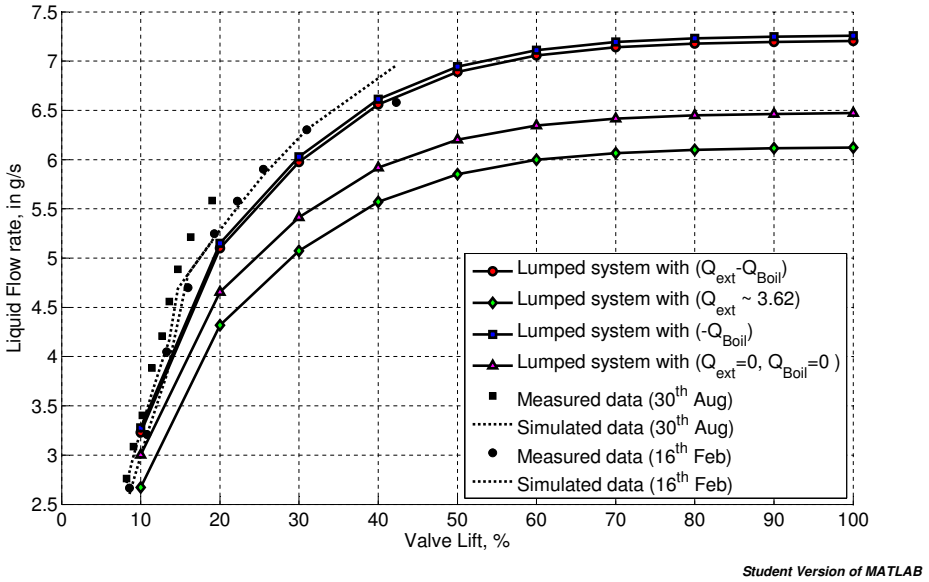

Figure 4: Liquid flow rates into the cryostat for various valve lift positions.

It is observed that the results obtained by incorporating the terms denoted here as $\dot{Q}_{boil}$ the external heat transfer rate in the energy balance equation agree the most with the measured data available from the process.

8.2.1 Sensitivity analysis: control valve chattering

Changes in the liquid flow rate due to changes in the control valve opening are investigated for valve openings of 1% around various valve opening values of $H = 0.1$ to $H = 0.9$. Table 14 gives the change in liquid flow rate due to a 1% change in valve opening at different mean operating valve positions.

It is clear that as the valve opens, the control on the liquid flow rate decreases; therefore the sensitivity of the liquid flow rate on the valve position also decreases. The sensitivity of the valve for lower valve openings causes instability in the numerical method based on the forward Euler time-stepping method, which is an explicit method.

Mean Valve Opening (H)	Mean Mass Liquid Flow Rate (L, in g/s)	Change in Liquid Flow Rate
0.10	3.23	26.09
0.20	5.10	10.01
0.30	5.98	7.34
0.40	6.56	4.43
0.50	6.89	2.35
0.60	7.06	1.15
0.70	7.14	0.55
0.80	7.18	0.25
0.90	7.20	0.12

Table 14: Sensitivity of liquid flow rate on 1% change in valve opening.

8.3 Heater step-input validation

The data from the heater step test are given in Table 15. Only the heater power input is required as input to the simulation along with the initial conditions. The cryostat pressure is regulated at 1.22 bars, and the level is regulated at 75%.

Time	Heater Power	Venturi Mass Flow (kg/s)	LHe Supply Valve Position (% open)	GHe Return Valve Position (% open)
0.00	80.25	5.72×10^{-3}	19.0	41.3
1020.00	69.50	5.34×10^{-3}	16.3	38.2
2340.00	57.78	5.01×10^{-3}	14.7	34.9
3660.00	50.49	4.68×10^{-3}	13.6	32.4
5400.00	40.89	4.33×10^{-3}	12.7	30.4
6360.00	30.89	4.00×10^{-3}	11.4	28.0
7380.00	20.47	3.52×10^{-3}	10.2	24.6
8700.00	9.62	3.19×10^{-3}	9.1	21.6
10320.00	0.00	2.87×10^{-3}	8.2	19.3

Table 15: Data for cryostat heater step test.

8.3.1 Comparison of numerical schemes

Due to the high sensitivity of the level control valve at low valve openings, the explicit forward Euler scheme suffers from numerical oscillations and is unstable. In Figure 5, the two plots compare the explicit forward Euler scheme with time step sizes dt = 0.5 s and dt = 0.25 s. It is seen that the

numerical oscillations develop later in time in the case of the smaller time step size, clearly indicating that they are non-physical in nature.

In Figure 6, we compare the explicit forward Euler and implicit backward Euler schemes for the same time step size. These plots illustrate the superior stability of implicit backward Euler scheme in spite of the extreme sensitivity of level control valve operation at low valve openings. In the light of this result, we use only the implicit schemes for other simulations.

In Figure 7, we compare the first-order implicit backward Euler scheme with the second-order implicit Crank–Nicolson scheme.

Figure 8 compares the pressure controller simulation based on the backward Euler and Crank–Nicolson schemes. Both schemes accurately predict the pressure in the cryostat as well as the valve position in controlling the pressure at a constant value. However, the second-order scheme suffers from the initial transient overshoot because it is slightly less stable.

As far as the gas mass flow rate from the cryostat is concerned, all the schemes perform equally well. This is because of the greater accuracy of the control-volume method in conserving quantities as compared to the finite-difference based discretization methods used in the 1D homogeneous model.

The circles indicate the times at which a change in heat power input is performed. The squares are the measured data obtained by running the cryostat in maintenance mode with different heater power inputs. The times and heater power input steps along with the gas mass flow rate and valve positions are noted in Table 15. The dotted line is the simulation result based on 1D homogeneous model using a linear correlation for static heat loading as a function of heater power input (as indicated in Figure 9). The dashed line is the simulation result based on 1D homogeneous model but using a constant value of static heat loading $\dot{Q}_s = 37.2$ W. The present simulation result is shown in the figure as a solid line.

8.4 Performance of the code

For steady-state simulations of the LHe transfer line, the previous code must complete transient calculations to converge to a steady-state solution, requiring approximately 200 to 300 s of wall clock time, depending on the valve opening. If only steady-state solutions are of interest yielding final liquid and gas flow rates into the cryostat, then the present code can give similar results in approximately 5 s. These timings are estimates only, obtained from simulations run on a machine with dual 2 GHz PowerPC G5 with memory of 1 GB DDR SDRAM. The codes are based on MATLAB 7.5 (R2007b) and run in the MAC OS X Version 10.5.8 operating system.

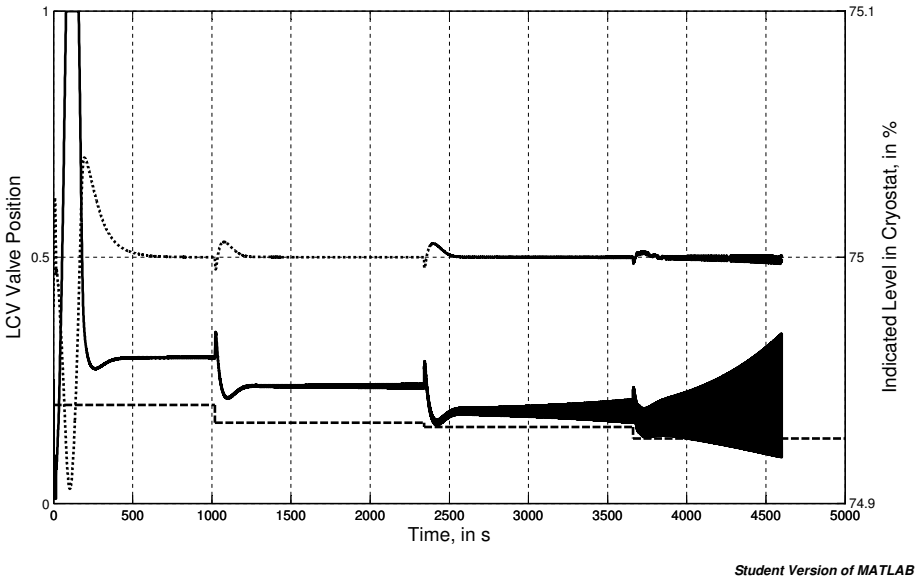

(a) Explicit scheme for dt = 0.50 s.

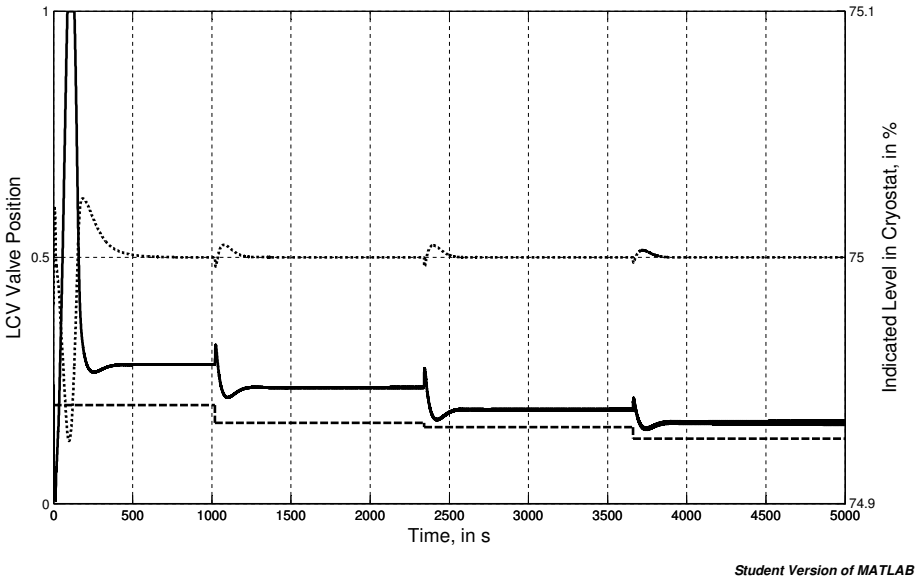

(b) Explicit scheme for dt = 0.25 s.

Figure 5: Comparison of explicit forward Euler method at time step sizes dt = 0.5 and 0.25 s for level control.

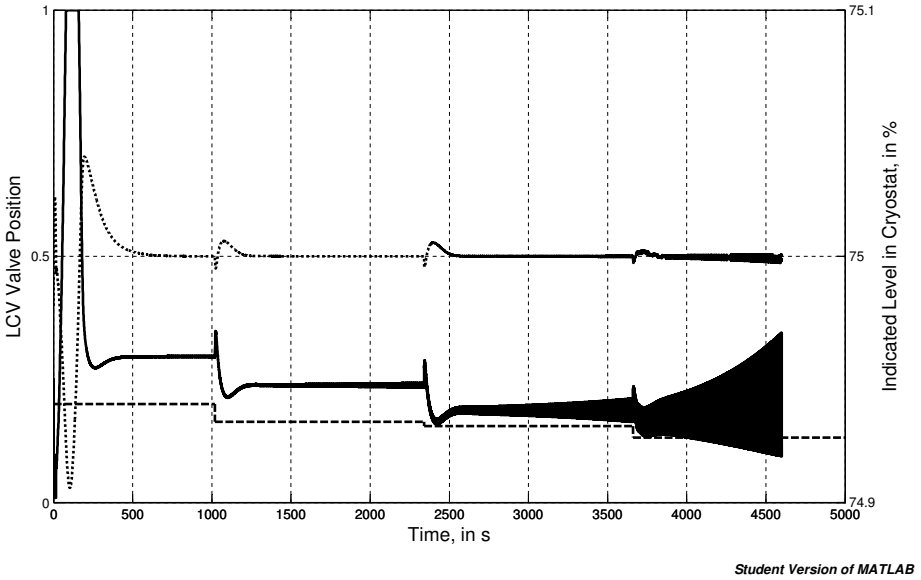

(a) Explicit Scheme for dt = 0.50 s.

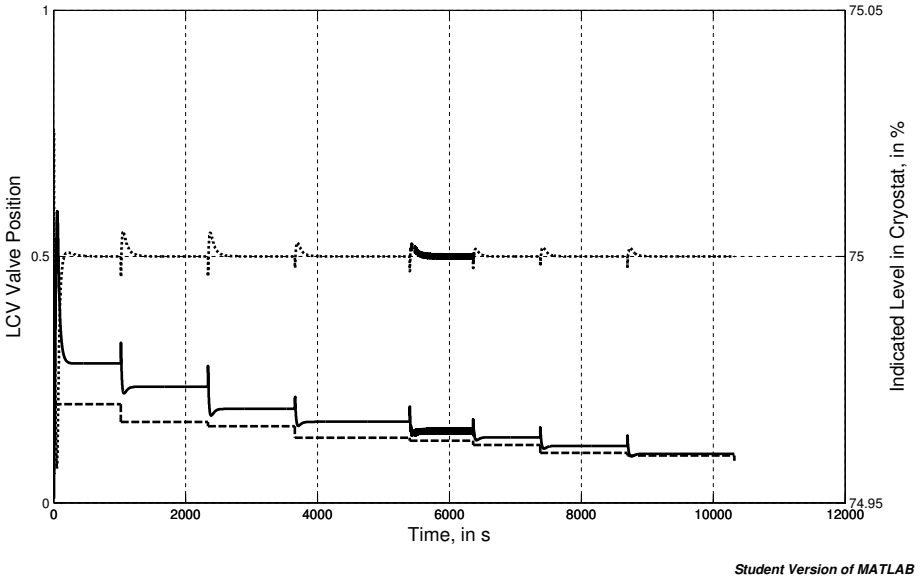

(b) Implicit Scheme for dt = 0.50 s.

Figure 6: Comparison of explicit forward Euler method and implicit backward Euler method at dt = 0.5 s for level control, illustrating the stability of the implicit scheme.

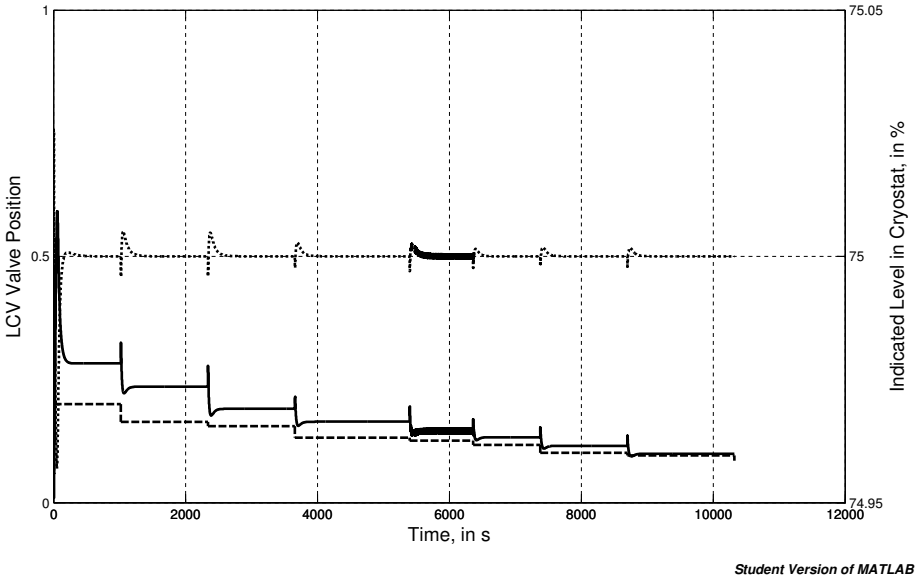

(a) First-order implicit method for dt = 0.50 s.

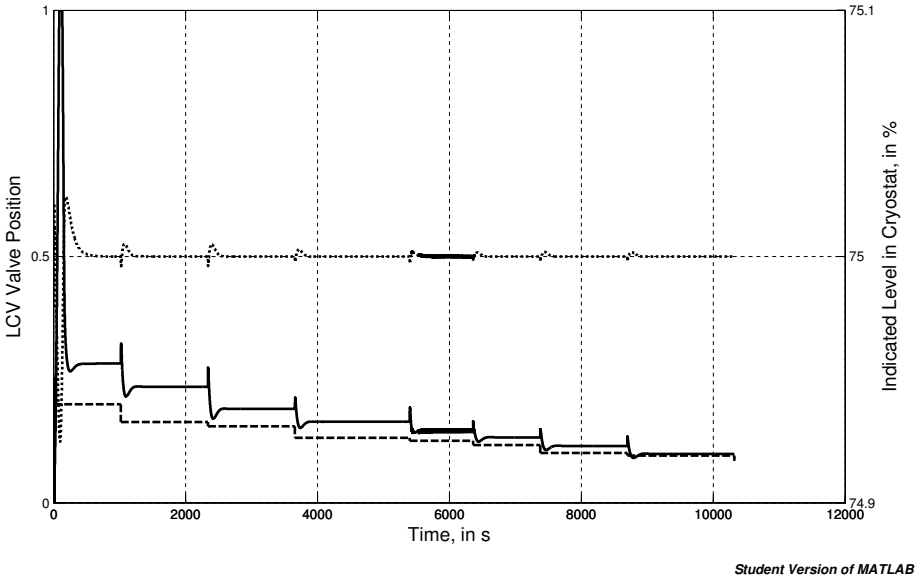

(b) Second-order implicit method for dt = 0.50 s.

Figure 7: Comparison of first-order implicit method and second-order implicit Crank–Nicolson method at dt = 0.5 s for level control.

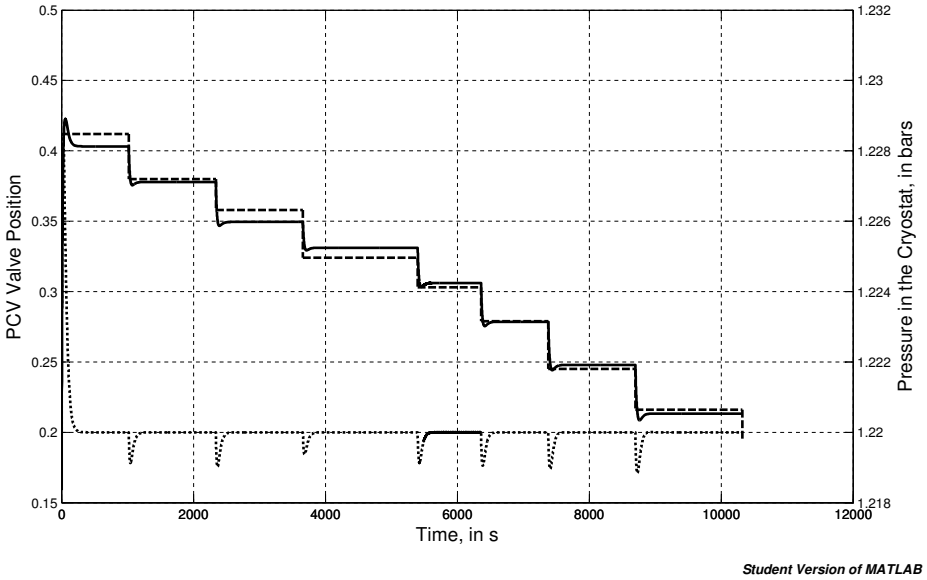

(a) First-order implicit for dt = 0.50 s.

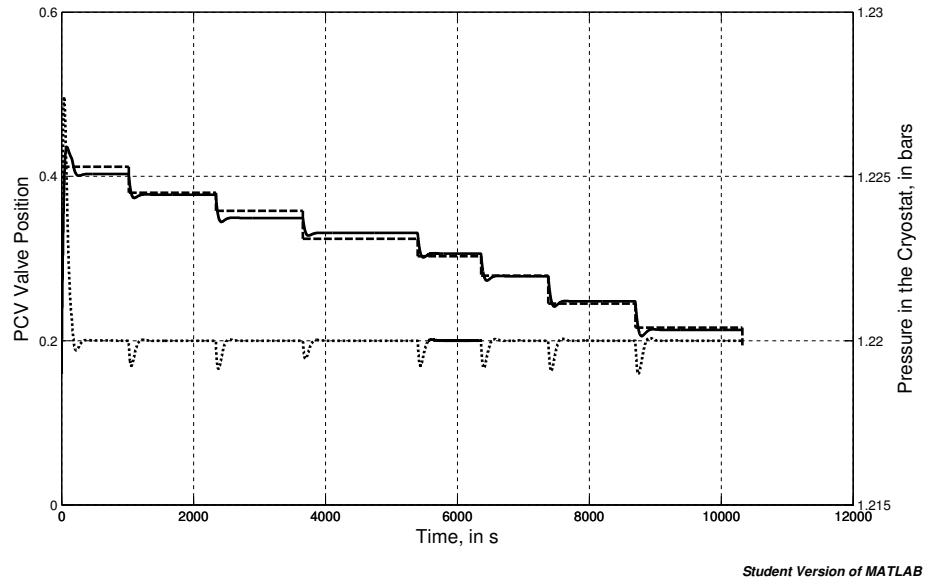

(b) Second-order implicit for dt = 0.50 s.

Figure 8: Comparison of first-order implicit method and second-order implicit Crank–Nicolson method at dt = 0.5 s for presssure control.

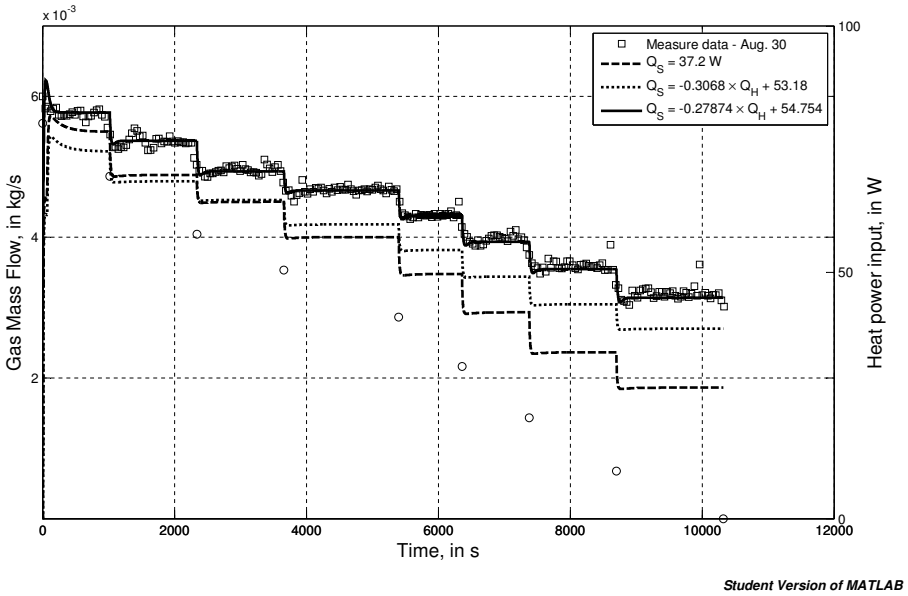

(a) First-order implicit method for dt = 0.50 s.

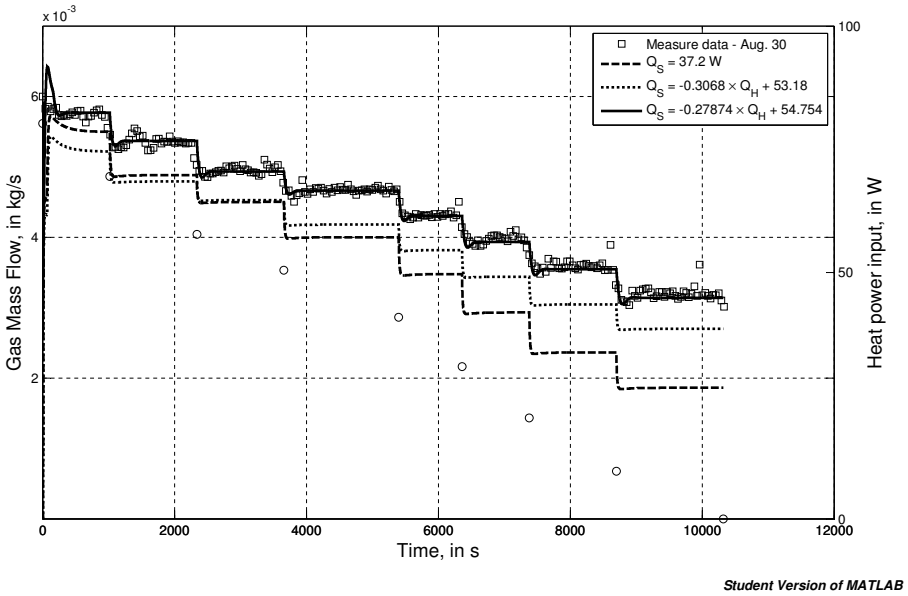

(b) Second-order implicit method for dt = 0.50 s.

Figure 9: Comparison of first- and second-order implicit methods for simulation of cryostat with time step size of dt = 0.5 s.

9 Conclusions

The current model of the cryogenic system at the CLS is based on one-dimensional, homogeneous model of two-phase flow of helium. The main contribution contained in this report is the development of a faster and more accurate computational method based on a control-volume approach. The faster computation of similar problem with respect to one dimensional homogeneous code and the two validations cases, viz., the liquid flow rate calculations versus different valve openings and the gas mass flow rate for heater power step test have proved the accuracy of the model and performance of the code.

The code is flexible in simulating varying lengths of the LHe line which can be used for calculations prior to process modifications.

The investigation of the physical meaning of an additional heat term $\dot{Q}_{boil}$ that accounts for better prediction of measured data needs to be performed. A heat of boiling term had already been proposed [6]; however this term is evaluated using an overall energy balance equation when two-phase formation occurs. In the present model, this term is used as an integral part of the overall energy balance. It is proposed that a part of the total energy of the system is used in creation of additional interfacial boundaries. The heat of boiling term evaluated through product of heat of vaporization and rate of gas formation seems to model this addition work done by the system well. When phase change occurs, the gas bubbles are formed either due to nucleation by cavitation (i.e. flashing of liquid due to reduction in pressure) or due to nucleation by boiling (i.e. flashing of liquid due to increase in temperature). After nucleation the bubbles of gas grows with further phase change. There is further work done by turbulence in breaking of bubbles. However, the homogeneous model may not be sufficient to capture this physics because the nucleation can occur in the fluid or at an solid-liquid interface. A more thorough model based on heterogeneous flow may be required to capture the interfacial physics.

The authors would like to acknowledge the help of Christopher Regier in discussions regarding the workings of the code based on the one-dimensional homogeneous model and for sharing the measured data used for validation of the present code. This work was funded jointly by NSERC, MITACS, Inc. and the Canadian Light Source, Inc. through the MITACS Accelerate Internship Program.

References

[1] R. B. Bird, W. E. Stewart, and E. N. Lightfoot. *Transport Phenomena*. John Wiley and Sons, New York., 1960.

[2] F. Incropera and D. DeWitt. *Fundamentals of Heat and Mass Transfer*. 4th edition, 1996.

[3] E. Lemmon, M. McLinden, and D. Friend. Thermophysical properties of fluid systems. *NIST Chemistry Webbook, NIST Standard Reference Database*, (69), 2008. Available at: NIST Webbook.

[4] Spirax Sarco Ltd. Control valve characteristics. 2010. Available at: Spirax Sarco.

[5] C. Regier, J. Pieper, and E. Matias. Dynamic modeling of a liquid helium cryostat at the canadian light source. 50:118–125, 2010.

[6] C. N. Regier. *Dynamic Modeling of a Cryogenic System at the Canadian Light Source*. PhD thesis, University of Calgary, Calgary, AB, Canada, 2009.

[7] The Engineering Toolbox. Emissivity coefficients of some common materials. 2010. Available at: The Engineering Toolbox.

[8] F. White. *Fluid Mechanics*. McGraw Hill Inc., New York., 1994.